Structure, Volume *21*

Supplemental Information

The Glove-like Structure of the Conserved Membrane Protein TatC Provides Insight into Signal Sequence Recognition in Twin-Arginine Translocation

Sureshkumar Ramasamy, Ravinder Abrol, Christian J.M. Suloway, and William M. Clemons, Jr.

Inventory of Supplemental Information

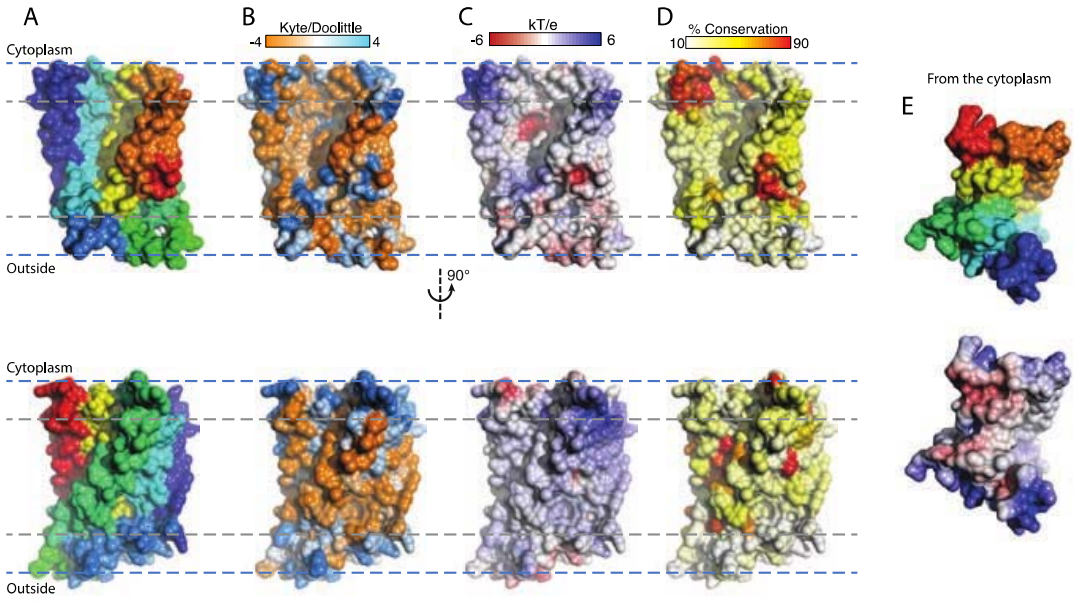

Figure S1, related to Figure 1: TatC surface representations.
(A-D) Front (*top*) and back (*bottom*) molecular surface representations: (A) colored as in Fig. 1*A*; (B) color based on the Kyte-Doolittle hydrophobicity scale from most apolar -4 (orange) to most polar 4 (cyan); (C) surface charge calculated based on electrostatic potential color scale from negative -6 kB/e (red) to positive +6 kB/e (blue); (D) surface conservation based on an alignment of TatC Pfam seed sequences color scale based on percent conservation from 10 (white) to 90 (red). (E) similar coloring to *A* and *C* viewed from the cytoplasm

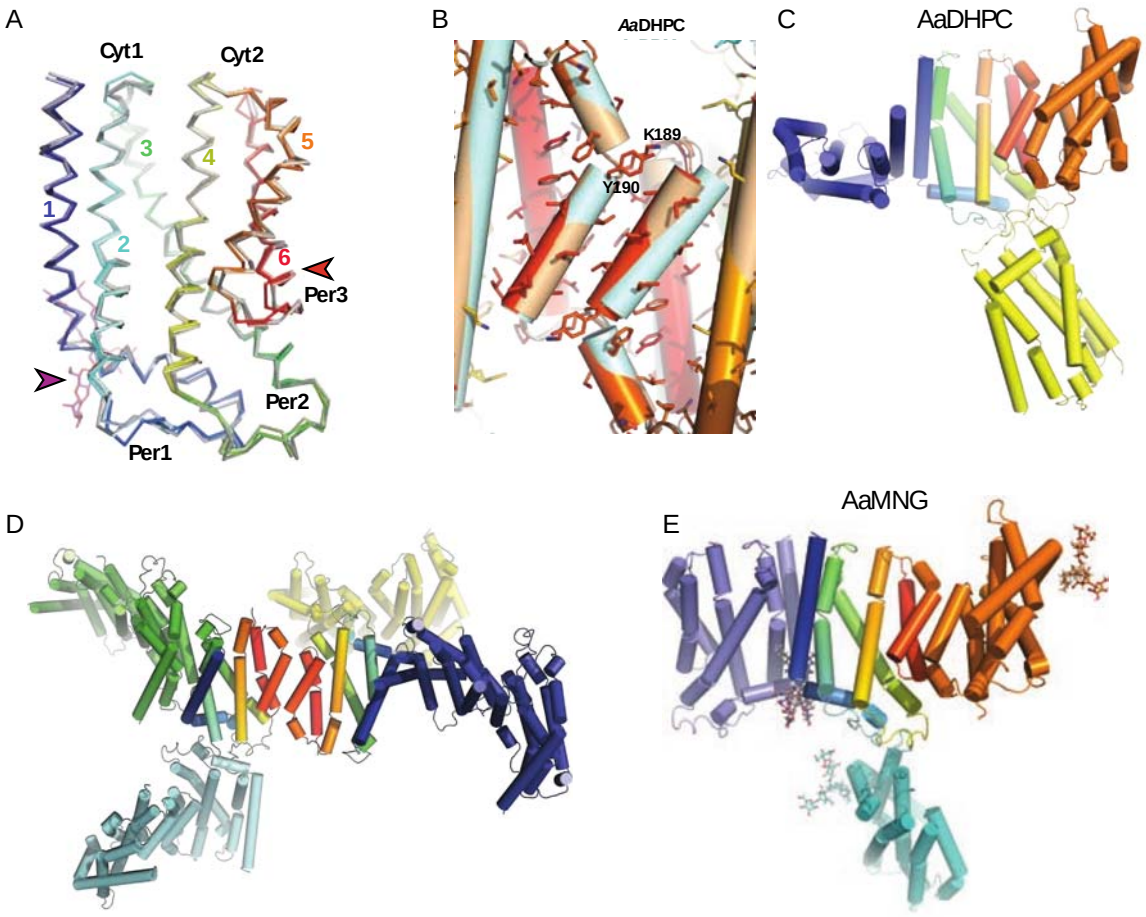

Figure S2, related to Figure 2: TatC structures and crystal packing.
(A) Cα trace of the three crystal structures with *Aa*DHPC (colored as in Fig. 1*A*), *Aa*DDM (lighter color similar to *Aa*DHPC) and *Aa*MNG (*gray*). The region of most variability (Per3) is highlighted by a red arrow. The bound detergent in *Aa*MNG is highlighted by a purple arrow. (B) A cartoon cylinder aligned to show the TM5 crystal packing. Structures are colored as noted in labeling with *Aa*DHPC as in *A*. Sidechains are shown as sticks. The structures are aligned to TM5 in the left TatC. (C-E) Significant crystal packing contacts in the *Aa*DHPC, *Aa*DDM, *Aa*MNG crystal forms, respectively. The asymmetric unit is shown as color ramped. Symmetry related contacts are colored relative to their primary contact to the asymmetric unit.

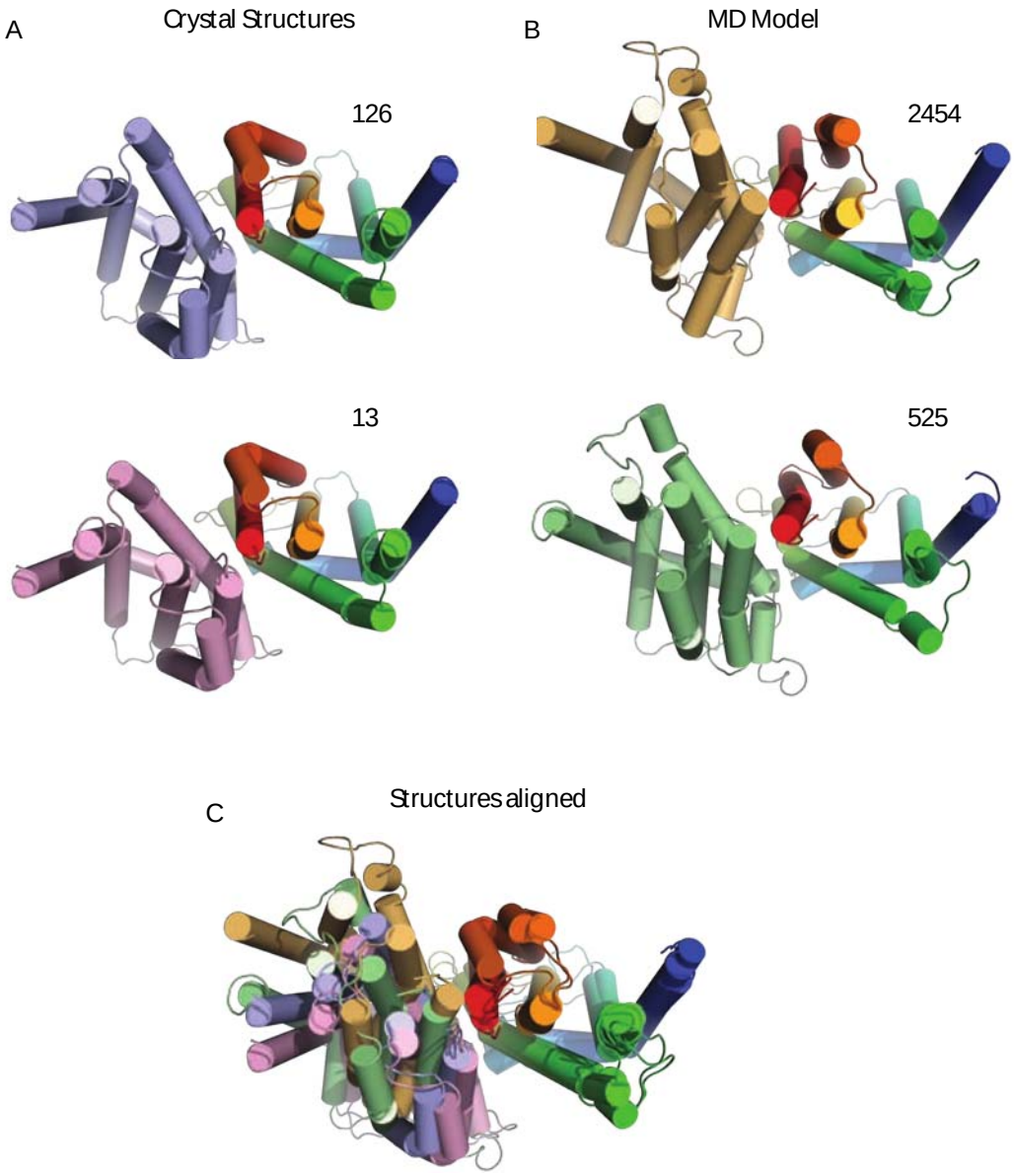

Figure S3, related to Figure 4: Dimer models of TatC.
Models are selected based on the top value in either energy scoring system and those that are highly ranked in both (Table S2). The number from the model name is displayed (Table S2). (A) Two models for the TatC dimer based on the *Aa*DHPC crystal structure. (B) Two models for the TatC dimer based on the MD model. (C) Alignment of the four structures to the color-ramped monomer.

Table S1. Top twenty energy rankings of 89 dimer models

Ranked by BE				Ranked by TE		
Rank	Model Name	**BE**	TE	Model Name	BE	**TE**
1	X-ray Model 13*	**-160**	797	MD Cluster #2 2454*	-78	**641**
2	X-ray Model 14	**-142**	795	MD Cluster #2 2937	-68	**652**
3	X-ray Model 99	**-135**	783	MD Cluster #3 2723	-67	**675**
4	X-ray Model 126*	**-134**	766	MD Cluster #3 2540	-61	**687**
5	X-ray Model 76	**-133**	774	MD Cluster #3 3039	-89	**710**
6	X-ray Model 251	**-125**	790	MD Cluster #3 525*	-101	**712**
7	X-ray Model 74	**-122**	798	MD Cluster #3 3872	-81	**731**
8	X-ray Model 35	**-120**	777	MD Cluster #3 3991	-62	**740**
9	X-ray Model 2236	**-120**	824	MD Cluster #3 1850	-48	**756**
10	X-ray Model 47	**-116**	864	X-ray Model 758	-79	**761**
11	X-ray Model 78	**-112**	821	X-ray Model 126*	-134	**766**
12	X-ray Model 1163	**-110**	797	MD Cluster #1 2396	-70	**768**
13	X-ray Model 65	**-109**	813	MD Cluster #3 729	-85	**768**
14	X-ray Model 385	**-106**	781	X-ray Model 3570	-79	**771**
15	X-ray Model 1770	**-104**	815	X-ray Model 1422	-95	**772**
16	X-ray Model 2971	**-104**	791	MD Cluster #1 1659	-24	**772**
17	X-ray Model 3153	**-104**	796	X-ray Model 76	-133	**774**
18	X-ray Model 891	**-101**	788	MD Cluster #1 2356	-65	**775**
19	MD Cluster #3 525*	**-101**	712	X-ray Model 3606	-43	**776**
20	X-ray Model 1654	**-101**	777	X-ray Model 1654	-101	**777**

Homodimer conformations common to the top 20 by both scoring energies

* models highlighted in Fig. S3

Supplemental Experimental Procedures

Deletion of native E. coli TAT genes in an expression strain

E. coli ΔtatABCDΔtatE expression strains were derived from BL21-Gold(DE3) (Stratagene) by a one-step gene inactivation (Cherepanov and Wackernagel, 1995). The region upstream of *tatA* was amplified by PCR from *E. coli* K-12 genomic DNA using the primers 5′-GGAAG TGCAG CCGCA ACTGG-3′ and 5′-CATAC ATGTT CCTCT GTGG-3′ while the region downstream of *tatD* was amplified using 5′-GCGTT TTAGA GTTTG CGGAA CTCG-3′ and 5′-CTATC CTTGC GCCCC GATTA AACGG-3′. The *tatABCD* flanking PCR products, along with the PCR products from the template plasmid pKD13, amplified using the homology extension PCR primers 5′-TGTGA AGAAT ACCGA GTTCC GCAAA CTCTA AAACG CGTGT AGGCT GGAGC TGCTTC-3′ and 5′-TGTTT AATCA TCATC TACCA CAGAG GAACA TGTAT GCTGT CAAAC ATGAG AATTA A-3′, were used to replace the *tatABCD* operon with a kanamycin resistance cassette to construct *ΔtatABCD::kan* as described in (Datsenko and Wanner, 2000). The kanamycin resistance cassette was removed by FLP recombinase to construct the *ΔtatABCD* strain using pCP20 which we refer to as CJMS1 (Cherepanov and Wackernagel, 1995). The *tatE* replacement kanamycin resistance cassette was amplified by PCR directly from the Keio collection (Baba et al., 2006) *ΔtatE766::kan* strain JW0622-1 using 5′-GGCGC GTTCT GTTGC CGGTT ATATG TCAAG AAGGT ATCTC TGTCA AACAT GAGAA TTAA-3′ and 5′-GTATC GAACA AGATA TTGAG GGAGC GTCCT GCTCG CCACG GTGTA GGCTG GAGCT GCTTC-3′. The amplified *ΔtatE766::kan* region was integrated into the CJMS1 strain and the kanamycin resistance cassette was removed (as described for the *tatABCD* deletion) to construct the *ΔtatABCDΔtatE* strain CJMS2.

Cloning, Expression and Purification

A codon optimized *Aa*TatC gene was synthesized based on the protein sequence by PCR primer extension using the DNAworks method (Hoover and Lubkowski, 2002). This was ligated into a modified pET33b expression vector (Novagen) using the SalI and BglI restriction sites resulting in a N-terminal 6xHis-tag. Mutants were generated using the quick-change method (Braman et al., 1996). A codon optimized C54T and C97A mutated T4-lysozyme was added to this plasmid using the MscI and BglI restriction sites with the added linker sequence of ASASG. For the rest of the work the proteins were essentially treated the same. Plasmids were transformed into the CJMS2 strain. Plated cells were inoculated directly into 12 L of 2xYT media containing 35 μg ml^{-1} kanamycin. Cultures were grown at 310 K to an OD600 of 0.4, then induced with 300 μM isopropyl β-D-1-thiogalactopyranoside (IPTG from Anatrace) for three hours. Cells were harvested by centrifugation and the pellet was 10-fold diluted in Buffer A (300 mM NaCl, 50 mM Tris HCl pH 7.5, glycerol 10% v/v) with 5 mM of β-mercaptoethanol, 0.1 mM phenylmethanesulphonylfluoride (PMSF) and protease inhibitors cocktail (Roche). Homogenized cells were lysed by passing three times though a microfluidizer M10L (Microfluidics). Cell debris was removed by low speed centrifugation at 13,000g for 30 minutes at 277K. The supernatant was collected and membranes were pelleted at 81,275*g* for 1 hr. The membrane fraction was harvested and incubated for 1 h in buffer A with 30 mM imidazole and 1% (w/v) dodecyl-β-d-maltopyranoside (DDM; Anatrace) at 4 °C. Another ultracentrifugation step at 36,122*g* for 30 min removed unsolubilized membrane components. The supernatant was loaded onto a gravity column containing 2.5 ml nickel-nitrilotriacetic acid-agarose beads (Ni-NTA) (Qiagen) pre-equilibrated and washed with 100 ml of buffer A including 30 mM imidazole and 0.03% (w/v) DDM, then eluted with buffer A containing 300 mM imidazole. The protein was concentrated using a centrifugal concentration device (Amicon ultra, Millipore) and dialyzed into phosphor-buffered saline (PBS) buffer including 10% glycerol and 0.03% DDM. The 6xHis-tag was cleaved with 20 units of thrombin incubated

overnight at 295K resulting in an additional four residues at the native N-terminus (GSVD). The remaining uncleaved protein was removed by passage over a second Ni-NTA affinity resin. The protein was concentrated using a centrifugal concentration device (Amicon ultra, Millipore) to about 5 mg ml^{-1} before further purification by gel filtration (Superdex-200 16/60; GE Healthcare) in buffer A containing 0.03% DDM. The peak fractions were collected and concentrated and the detergent was exchanged into 0.1% DHPC in Buffer A over a Superdex-200 10/300 column (GE Healthcare) then concentrated to 15 mg ml^{-1} and flash-frozen in liquid nitrogen.

Crystallization and Structural Determination

Extensive crystallization trials were performed for *Aa*TatC purified in various detergents. The *Aa*TatC protein, with a final concentration of ~18 mg/ml, purified in 0.1% DHPC (*Aa*DHPC) gave rise to crystals in multiple poly-ethylene glycol (PEG) conditions. Typical crystals were grown in a hanging-drop format over a reservoir solution of 25-30% Jeffamine ED-2001, 50 mM HEPES pH 7.5 and 10% (v/v) methyl-2,4-pentanediol (MPD). Crystals were flash frozen and stored in liquid nitrogen with 15% MPD added to the reservoir solution as cryoprotectant. The initial crystals from DHPC did not diffract; however, simple optimization resulted in spots visible at ~10Å resolution. To improve these, mutants were generated to reduce surface entropy with one combination (K40A, E41A and a C-terminal truncation) resulting in well-formed crystals that diffracted to 7.5 Å. Upon visual inspection, it became clear that two distinct crystal forms were growing in the same drop. The less common of the two forms diffracted better; therefore, one of these crystals was used to microseed into clear drops resulting in only this form appearing. From this a single crystal was obtained that diffracted to high resolution and was used to collect a native dataset at 4.0Å resolution (*Aa*DHPC). Subsequent further preparations of the protein with newly purchased DHPC failed to produce similar results. Comparing to the preparation that resulted in the high-resolution crystal, it became clear that there were differences in the detergent

batches (*e.g.* different elution profiles by gel filtration). Unfortunately, we were unable to identify the nature of the differences at the chemical level.

An alternative approach to obtain high-resolution crystals was to generate a lysozyme-*Aa*TatC fusion similar to that used for GPCR crystallization (Rosenbaum et al., 2007). A codon optimized T4 lysozyme gene was either inserted between residues 44 to 55 in the first periplasmic loop or appended to the C-terminus. The C-terminal lysozyme version expressed similar to the wild-type protein while the insertion expressed poorly. Both fusions were well behaved by gel filtration and were put into crystallization trials. Only the C-terminal fusion resulted in crystals. The final *Aa*TatC plus lysozyme in DDM (*Aa*DDM) crystallized in 35% (v/v) PEG 400, ADA pH 6.6 and 0.1 M potassium phosphate monobasic. Crystals grew to full size within 10 to 14 days and were flash frozen in liquid nitrogen without additional cryoprotectant.

Images were collected at SSRL beamline 12-2 on a Mar Mosaic-325 CCD detector. Diffraction data were integrated either with XDS (Kabsch, 2010) or Mosflm (Battye et al., 2011) and scaled with SCALA in the CCP4 suite (Winn et al., 2011). The *Aa*DHPC crystals were in the $P4_122$ space group with unit cell dimensions a=b=110.43 c=107.43 and a complete dataset was collected to 4.0 Å. The asymmetric unit contained one TatC monomer. The *Aa*DDM crystals were in the space group $I4_122$ with the cell dimensions a=b=142.02 c=251.75 and a complete data set was collected to 6.8 Å. This asymmetric unit contains two monomers. All crystallographic statistics are provided in Table 1.

The phases for both crystal forms were solved by molecular replacement using the structure PDBID 4B42 of *Aa*TatC minus the bound detergent as a search model (space group H32) in PHASER with default parameters as implemented in Phenix (McCoy, 2007); (Adams et al., 2010). Model rebuilding was performed using Coot (Emsley et al., 2010). *Aa*DHPC was refined in Phenix using group B-factors and secondary structure restraints while *Aa*DDM was refined using the CNS DEN method

(Schroder et al., 2010). The validation of the final structural models were performed using Molprobility (Chen et al., 2010).

Multi-Angle Laser Light-Scattering Analysis

Purified *Aa*TatC in DDM (15 mg/ml) was loaded onto a Shodex protein KW-803 size-exclusion column equilibrated with 50 mM Tris-HCl pH 7.5, 100 mM NaCl, 0.03 % (v/w) DDM and connected in-line with a Dawn 18-angle light-scattering detector coupled to an Optilab interferometric refractometer and a WyattQELS (Quasi-Elastic Light-Scattering instrument) (Wyatt Technologies). Data analysis was performed with the ASTRA V5.3.4.04 software (Wyatt Technologies) and molecular weights were calculated using the Zimm fit method.

Setup of the protein-lipid system for molecular dynamics

The TatC protein structure was first aligned in an implicit membrane using the OPM server (Orientation of Proteins in Membranes (Lomize et al., 2006)) to orient the protein in the *xy*-plane, such that the z=0 plane corresponds to middle of the membrane bilayer. This oriented complex was then placed in a 1-palmitoyl 2-oleoyl phosphatidylcholine (POPC) lipid-bilayer block of cross-section 75 Å × 75 Å in the *xy*-plane, with the cytoplasmic side of the protein facing the $-z$ direction. POPC was chosen as it is commonly used in these types of experiments and previous studies suggest that the choice of lipid head group had minimal effects on a standard simulation (Pantano and Klein, 2009). The distance between the layers and surface density of lipid molecules were chosen to match those from experiments (Rand and Parsegian, 1989). The phosphatidylcholine headgroup is solvated and some disorder is built into the lipid bilayer patch to get the starting structure closer to the real lipid environment. This system is then sandwiched between two blocks of size 75 Å × 75 Å × 15 Å containing pre-equilibrated water molecules. Any lipid or water molecules overlapping with the protein are eliminated. The system is then neutralized by adding the required numbers of sodium or chloride ions that are placed randomly in the

system but avoiding any clashes. This whole setup procedure is implemented using the VMD (Visual Molecular Dynamics) package (Humphrey et al., 1996).

Molecular dynamics simulations

Parameters The simulations were carried out using NAMD (Phillips et al., 2005), a parallel MD code designed for computationally demanding biomolecular systems. The CHARMM force field (Brooks et al., 2009) was used for the protein and lipids while the TIP3P potential function parameterization (Jorgensen et al., 1983) was used for water molecules. NAMD employs periodic boundary conditions to remove surface effects. The resulting periodicity was used to calculate full electrostatic interactions using the particle-mesh Ewald summation method (Darden et al., 1993). The long-range electrostatic and van der Waals interactions were cutoff at 12 Å in the simulations. The calculations were performed under isothermal-isobaric conditions (NPT) at 310 K and 1 atm. The temperature was controlled using Langevin dynamics (with a coupling coefficient of 5 ps^{-1}) and the pressure was maintained using a Langevin-Hoover barostat (Quigley and Probert, 2004). A time step of 1 fs was used throughout this study.

Simulations The dynamics was carried out in 4 steps: first, lipid and water atoms were minimized for 5000 steps keeping the protein atoms fixed. This allowed for the lipids and waters to remove any bad contacts with each other and the protein. In the second step, the lipid and water atoms are equilibrated under NPT conditions (310K and 1atm) for 500 ps, while still keeping the protein atoms fixed. This let the lipids and waters relax in the presence of the protein and fill any gaps created during the system setup. Next, the full system (protein-lipid-water) was minimized for 5000 steps, allowing the protein atoms to adjust to the equilibrated lipids and waters. In the last step, the full system was equilibrated for 50.25 ns (50,250,000 time steps) under NPT conditions, of which the last 50 ns was used for analysis. Snapshots were saved every 10 ps.

Homodimer structure prediction

Protein-protein docking calculations were performed using the ZDock program (Chen et al., 2003). Protein-protein docking is challenging, where there are two major challenges: accounting for protein flexibility and the availability of an accurate scoring energy capable of correctly ranking protein-protein conformations. The latter is implemented using the all-atom Dreiding force field (Mayo et al., 1990).

Protein flexibility was tackled in two steps. In the first step, distinct protein-backbone conformations were obtained from clustering protein snapshots from the MD trajectory sampled (for clustering) every 0.5ns. These snapshots were clustered at 2 Å diversity using the K-means clustering method implemented in the MMTSB toolset (Feig et al., 2004) resulting in 3 clusters. Snapshots closest to the centroid (based on Cα-RMSD) of each cluster were picked to represent those clusters. Four protein conformations (three (M1, M2, M3) using the cluster heads from the MD trajectory and one (C1) using the crystal conformation) were used as input in four different protein-protein docking implementations. The second step of implementing protein flexibility involved side-chain flexibility. This was carried out by replacing (in the input protein conformations) larger hydrophobic residues (F, I, L, M, W, Y) with valines and larger polar residues (D, E, H, K, Q, R) by asparigines. Remaining residues were left unchanged in these "hydropathically coarsened" proteins. This preserved the hydropathic character of the protein surfaces, while allowing them to approach each other as close as possible and not be dependent on arbitrary conformations of larger amino acid side-chains.

These coarsened proteins (M1c, M2c, M3c, and C1c) were individually docked to their copies using the ZDock program with the fine sampling grid. 4000 protein-protein conformations were generated for each of the starting protein conformations. Many of these homodimer conformations were not compatible with the membrane bilayer boundary conditions and these were filtered out using a simple topological constraint. In the remaining 89 homodimer conformations, the original protein residues are inserted and all residues optimized using SCREAM (Kam and Goddard, 2008). This lead to

all protein side-chains being optimized specifically for each homodimer conformation. The resulting homodimers were minimized and ranked based on inter-protomer energies (BE) and total energies (TE) (Table S2). TE was calculated as the energy of the full homodimer using the all-atom Dreiding FF. BE is the binding energy between the two protomers in the homodimer. The energy terms TE and BE are related by: TE = E1+E2+BE where, E1 and E2 are the total energies of the isolated protomers.

Structure Analysis and Figures

Cartoon representations of protein structures were prepared using PyMol (Schrodinger, LLC), while surface representations were prepared using UCSF Chimera (Pettersen et al., 2004). Surface hydrophobicity was determined in Chimera using the Kyte-Doolittle scale (Kyte and Doolittle, 1982) for individual residues. Electrostatic surface potentials were calculated using APBS with default values as implemented in the PDB2PQR webserver (Baker et al., 2001; Dolinsky et al., 2004).

Supplemental References

Adams, P.D., Afonine, P.V., Bunkoczi, G., Chen, V.B., Davis, I.W., Echols, N., Headd, J.J., Hung, L.W., Kapral, G.J., Grosse-Kunstleve, R.W.*, et al.* (2010). PHENIX: a comprehensive Python-based system for macromolecular structure solution. Acta. Cryst. D*66*, 213-221.

Baba, T., Ara, T., Hasegawa, M., Takai, Y., Okumura, Y., Baba, M., Datsenko, K.A., Tomita, M., Wanner, B.L., and Mori, H. (2006). Construction of Escherichia coli K-12 in-frame, single-gene knockout mutants: the Keio collection. Mol. Syst. Biol. *2*, 2006-2008.

Baker, N.A., Sept, D., Joseph, S., Holst, M.J., and McCammon, J.A. (2001). Electrostatics of nanosystems: application to microtubules and the ribosome. Proc. Natl. Acad. Sci. USA *98*, 10037-10041.

Battye, T.G., Kontogiannis, L., Johnson, O., Powell, H.R., and Leslie, A.G. (2011). iMOSFLM: a new graphical interface for diffraction-image processing with MOSFLM. Acta Cryst. D*67*, 271-281.

Braman, J., Papworth, C., and Greener, A. (1996). Site-directed mutagenesis using double-stranded plasmid DNA templates. Methods Mol. Biol. *57*, 31-44.

Brooks, B.R., Brooks, C.L., 3rd, Mackerell, A.D., Jr., Nilsson, L., Petrella, R.J., Roux, B., Won, Y., Archontis, G., Bartels, C., Boresch, S.*, et al.* (2009). CHARMM: the biomolecular simulation program. J. Comp. Chem. *30*, 1545-1614.

Chen, R., Li, L., and Weng, Z. (2003). ZDOCK: an initial-stage protein-docking algorithm. Proteins *52*, 80-87.

Chen, V.B., Arendall, W.B., 3rd, Headd, J.J., Keedy, D.A., Immormino, R.M., Kapral, G.J., Murray, L.W., Richardson, J.S., and Richardson, D.C. (2010). MolProbity: all-atom structure validation for macromolecular crystallography. Acta Cryst. D*66*, 12-21.

Cherepanov, P.P., and Wackernagel, W. (1995). Gene disruption in Escherichia coli: TcR and KmR cassettes with the option of Flp-catalyzed excision of the antibiotic-resistance determinant. Gene *158*, 9-14.

Darden, T., York, D., and Pedersen, L. (1993). Particle mesh Ewald - an N.Log(N) method for Ewald sums in large systems. J. Chem. Phys. *98*, 10089-10092.

Datsenko, K.A., and Wanner, B.L. (2000). One-step inactivation of chromosomal genes in Escherichia coli K-12 using PCR products. Proc. Natl. Acad. Sci. USA *97*, 6640-6645.

Dolinsky, T.J., Nielsen, J.E., McCammon, J.A., and Baker, N.A. (2004). PDB2PQR: an automated pipeline for the setup of Poisson-Boltzmann electrostatics calculations. Nucl. Acids Res. *32*, W665-667.

Emsley, P., Lohkamp, B., Scott, W.G., and Cowtan, K. (2010). Features and development of Coot. Acta Cryst. D*66*, 486-501.

Feig, M., Karanicolas, J., and Brooks, C.L., 3rd (2004). MMTSB Tool Set: enhanced sampling and multiscale modeling methods for applications in structural biology. J. Mol. Graph. Model *22*, 377-395.

Hoover, D.M., and Lubkowski, J. (2002). DNAWorks: an automated method for designing oligonucleotides for PCR-based gene synthesis. Nucl. Acids Res. *30*, e43.

Humphrey, W., Dalke, A., and Schulten, K. (1996). VMD: visual molecular dynamics. J. Mol. Graph. *14*, 33-38, 27-38.

Jorgensen, W.L., Chandrasekhar, J., Madura, J.D., Impey, R.W., and Klein, M.L. (1983). Comparison of simple potential functions for simulating liquid water. J. Chem. Phys. *79*, 926-935.

Kabsch, W. (2010). XDS. Acta Cryst. D*66*, 125-132.

Kam, V.W.T., and Goddard, W.A. (2008). Flat-Bottom Strategy for Improved Accuracy in Protein Side-Chain Placements. J. Chem. Theory Comput. *4*, 2160-2169.

Kyte, J., and Doolittle, R.F. (1982). A Simple Method for Displaying the Hydropathic Character of a Protein. J. Mol. Biol. *157*, 105-132.

Lomize, M.A., Lomize, A.L., Pogozheva, I.D., and Mosberg, H.I. (2006). OPM: Orientations of proteins in membranes database. Bioinformatics *22*, 623-625.

Mayo, S.L., Olafson, B.D., and Goddard, W.A. (1990). Dreiding - a Generic Force-Field for Molecular Simulations. J. Phys. Chem. *94*, 8897-8909.

McCoy, A.J. (2007). Solving structures of protein complexes by molecular replacement with Phaser. Acta Cryst. D*63*, 32-41.

Pantano, D.A., and Klein, M.L. (2009). Characterization of membrane-protein interactions for the leucine transporter from Aquifex aeolicus by molecular dynamics calculations. J. Phys. Chem. B *113*, 13715-13722.

Pettersen, E., Goddard, T., Huang, C., Couch, G., Greenblatt, D., Meng, E., and Ferrin, T. (2004). UCSF Chimera--a visualization system for exploratory research and analysis. J. Comput. Chem. *25*, 1605-1612.

Phillips, J.C., Braun, R., Wang, W., Gumbart, J., Tajkhorshid, E., Villa, E., Chipot, C., Skeel, R.D., Kale, L., and Schulten, K. (2005). Scalable molecular dynamics with NAMD. J. Comput. Chem. *26*, 1781-1802.

Quigley, D., and Probert, M.I. (2004). Langevin dynamics in constant pressure extended systems. J. Chem. Phys. *120*, 11432-11441.

Rand, R.P., and Parsegian, V.A. (1989). Hydration forces between phospholipid-bilayers. Bioch. Biophys. Acta *988*, 351-376.

Rosenbaum, D., Cherezov, V., Hanson, M.A., Rasmussen, S.G., Thian, F., Kobilka, T., Choi, H., Yao, X.J., Weis, W., Stevens, R.C.*, et al.* (2007). GPCR engineering yields high-resolution structural insights into β2-adrenergic receptor function. Science *318*, 1266-1273.

Schroder, G.F., Levitt, M., and Brunger, A.T. (2010). Super-resolution biomolecular crystallography with low-resolution data. Nature *464*, 1218-1222.

Winn, M.D., Ballard, C.C., Cowtan, K.D., Dodson, E.J., Emsley, P., Evans, P.R., Keegan, R.M., Krissinel, E.B., Leslie, A.G., McCoy, A.*, et al.* (2011). Overview of the CCP4 suite and current developments. Acta Cryst. D*67*, 235-242.